

Template free large scale synthesis of multi-shaped ZnO nanostructures for optical, photocatalytical and antibacterial properties

A. N. Kadam¹ · R. S. Dhabbe¹ · M. R. Kokate¹ · N. L. Gavade¹ · P. R. Waghmare² · K. M. Garadkar¹

Received: 13 May 2015 / Accepted: 15 July 2015 / Published online: 19 July 2015
© Springer Science+Business Media New York 2015

Abstract In this article, ZnO nanostructures with diverse morphologies have been synthesized via a simple, rapid and cost effective solid state thermal decomposition method. The as-synthesized ZnO nanostructures were characterized by means of X-ray diffraction (XRD), Fourier transform infrared spectroscopy, scanning electron microscope (SEM), high-resolution transmission electron microscope (HR-TEM), UV–Vis. diffuse reflectance spectra (UV–Vis-DRS) and photoluminescence (PL). The XRD patterns and HR-TEM image indicated a hexagonal wurtzite structure of ZnO. The SEM images of ZnO samples show the different morphologies such as nanowire, nanorods, spherical and irregular microsphere at different calcination temperatures. Room temperature PL spectra of the samples exhibited characteristics blue and green emission bands in accordance with calcination temperature. Moreover, photocatalytic as well as antimicrobial activities were evaluated using ZnO synthesized at different calcination temperatures. The effects of calcination temperature, catalyst loading and pH on the photodegradation efficiency were systematically studied. A highest (99 %) photocatalytic activity of ZnO nanorods towards the Acid Green 25 (AG-25) was achieved within 35 min at optimal conditions under UV light. As-synthesized ZnO nanorods are found to be more efficient than TiO₂ (P25) towards the degradation of AG-25. It was found that the antimicrobial activity of ZnO nanorods (13 nm) obtained at 300 °C

showed significantly higher inhibition efficiencies than the other samples. The mineralization of AG-25 was confirmed from a reduction of 85 % the chemical oxygen demand within 35 min. In addition, ZnO nanorods could be easily reusable up to four runs without changing its photocatalytic activity.

1 Introduction

The release of dye effluents from textile and photographic industries into water bodies are becoming a major source of water pollution due to complex aromatic molecular structure of dyes which makes them more stable, resistance to chemical, photochemical and biological degradation [1]. The anthraquinone dye has been applied widely in the printing and dyeing industries due to its bright color, high fixation and good color fastness [2]. These dyes have low biodegradability, therefore conventional and biological processes are not much effective for the treatment of wastewater containing dye [3]. To overcome these problems, an environment friendly heterogeneous photocatalysis has emerged as a promising technology [4]. Moreover, it has many advantages such as high efficiency, energy saving, low running cost and no requirement of secondary treatment [5]. Although, TiO₂ is the most commonly used as an efficient photocatalyst for a wide range of organic pollutants [6]. ZnO has been another suitable semiconductor recognized as a promising photocatalyst, since its band gap and photodegradation mechanism have been proven to be similar to TiO₂ [7]. There are several advantages of ZnO in comparison with TiO₂ such as, it absorbs large fraction of UV light, large exciton binding energy (60 meV), more quantum efficiency, high photocatalytic activity, low production cost, easy availability and

✉ K. M. Garadkar
kmg_chem@unishivaji.ac.in

¹ Nanomaterials Research Laboratory, Department of Chemistry, Shivaji University, Kolhapur 416004, India

² Department of Bio-Chemistry, Shivaji University, Kolhapur 416004, India

environment friendly [9]. In a few cases, ZnO was also reported as an efficient photocatalyst than TiO₂ [8].

The inorganic nanomaterials have attracted considerable attention because of strong antimicrobial activity at lower concentration [10]. Among the inorganic materials, metal oxide nanoparticles are of special interest due to their efficient antimicrobial activity under extreme conditions, such as at high temperature and pressure [11]. The unique antimicrobial activity of ZnO nanostructure in dark and light has also attracted significant research interest owing to its unique morphology [12]. In particular, it has been demonstrated that the photocatalytic and antimicrobial activity of ZnO nanostructures are strongly dependent on the crystallite size, surface area, morphology and surface texture [13–15]. Therefore number of studies were carried out on the preparation of ZnO nanostructures with different morphology [16, 17]. A variety of physical and chemical methods have been successfully employed to fabricate different ZnO nanostructures in various shapes [18]. However, some physical methods always need more expensive, sophisticated instrumentation and complex procedures [19]. In case of solution method, preparation procedure is relatively complex, associated with toxic and expensive reagents with a lower concentration of reagents, thus leading to low yield of the desired product [20]. All of these factors limit their practical applications of ZnO based photocatalyst in an actual application. Although many synthetic routes have been extensively tried for the preparation of one-dimensional ZnO nanostructures, the development of a facile and efficient one-step route to synthesize a large-scale ZnO nanostructure remains a challenge. Compared to other, solid state based thermal decomposition process has no limit of reagent concentration, thus allows for a large scale synthesis of nanomaterials [21].

In the present work, ZnO nanostructure with different morphologies such as, nanowires, nanorods, spherical and irregular microsphere have been synthesized by a simple thermal decomposition method which is an economically favorable, rapid and applicable to large scale production. The plausible growth mechanism of change in morphology with temperature was also discussed. To the best of our knowledge, this is the first detailed investigation of photocatalytic degradation of the AG-25 under UV (365 nm) illumination was carried out by using ZnO as a photocatalyst. In order to achieve maximum photodegradation of AG-25, the effect of various parameters such as calcination temperature, catalyst loading and initial pH of the dye solution have been optimized systematically. The mineralization of AG-25 was confirmed by monitoring chemical oxygen demand (COD) of photodegraded product. The photodegraded intermediate products were identified using LC–MS. We have also studied the antimicrobial activity of

ZnO nanostructures against *E. coli*. This work demonstrates that as-synthesized ZnO nanostructures play an important role in photocatalytic as well as antimicrobial activity due to their various morphology.

2 Experimental

2.1 Materials and methods

Zinc acetate dihydrate [Zn(AC)₂] (99.5 % s d fine-chemical Ltd.) used in the present study was analytical grade and used as received. AG-25 was purchased from Aldrich chemicals. Zn(AC)₂ was used as the starting material for the synthesis of ZnO nanostructures. In a typical synthesis, 6.0 g of Zn(AC)₂ was taken in the mortar and pestle, then grounded well for 1 h, finally this powder was calcined in silica crucible at a different calcination temperatures (300, 400, 600 and 800 °C) for 3 h and then allowed to cool.

2.2 Characterization of ZnO samples

Thermal stability of Zn(AC)₂ was tested by using TGA-DTA instrument, (SDT Q600V20.9 Build 20TA Instruments, USA) under N₂ atmosphere. XRD of as-synthesized ZnO was recorded on a Panalytical diffractometer with Cu K α radiation ($\lambda = 1.5406 \text{ \AA}$) in the range of 2θ , 10–80°. Fourier transform infrared spectra (FT-IR) of ZnO were recorded on the Spectrum-one (Perkin Elmer) in the range of 4000–400 cm⁻¹ using KBr pellet. The UV–Vis. diffuse reflectance spectra were recorded on spectrophotometer (Varian Cary-5000 UV–Vis.-NIR). Photoluminescence of the sample was recorded on Spectrofluorimeter (JASCO, Model F.P.750 Japan). The surface morphology and composition of ZnO nanostructures were scanned by scanning electron microscope (SEM) (JEOL, JSM-6360) attached with EDS at various magnifications. The transmission electron microscopy (TEM) images were scanned by TEM (Equipped with high resolution Gatan CCD camera). The degradation products of dye tested on LC–MS equipped with electron spray Ionization Interface (Shimadzu, Japan).

2.3 Photocatalytic activity of ZnO nanostructures

The photocatalytic activity of ZnO was evaluated for the degradation of AG-25 under UV light (365 nm). To evaluate optimal photocatalytic activity of ZnO nanostructure, the amount of photocatalyst was varied from 0.5 to 2 g/dm³ in AG-25(25 ppm). The effect of pH on the photocatalytic activity was studied by adjusting pH of solution from 3 to 11 using HCl and NaOH (1 M each). Typically, in this experiment photocatalyst was added in a photo-reactor containing 100 mL of AG-25. Before the irradiation of

light, the dye solution was stirred for 30 min in the dark to ensure an adsorption–desorption equilibrium, then the dye solution was exposed to light. All photodegradation experiments were performed at ambient temperature. At a given time interval, aliquots were collected from a photo-reactor and centrifuged to remove smaller particles of the photocatalyst. The centrifuged solution was used to monitor change in the concentration of AG-25 by recording the absorbance at λ_{max} 643 nm by using UV–Vis.-NIR spectrophotometer. COD of the irradiated solution was used to monitor the mineralization of the AG-25 using the open reflux titrimetric method [22].

2.4 Antimicrobial activity

The ZnO nanostructures were synthesized by thermal decomposition method with different morphology such as nanowires, nanorods, spherical and micro size irregular sphere. The antimicrobial activity of as-synthesized ZnO nanostructures was determined by pour plate agar well diffusion method in which the target pathogenic organism *E. coli* (ATCC 25922) was used. The *E. coli* was cultured in 5 mL nutrient broth for 24 h at 30 °C under shaking growth condition. The freshly grown *E. coli* was aseptically added to the autoclaved nutrient agar (1.5 % media) at 40 °C. After the solidification of media into the sterile petridish, it was punctured by using a flame sterilized stainless steel cork borer. The test solution of ZnO (1 mg/mL) was used as stock which is aseptically (100 μ L) loaded into the 6 mm well punctured in the media with dilution 1:1, 1:2 and 1:3. The plates were incubated for 15 min. at 4 °C to ensure the diffusion of compound of interest into the media. After which the plates were incubated for 24 h at 30 °C in microbial incubator. Zones of inhibition were measured at the end of the incubation period.

3 Results and discussion

3.1 TGA-DTA of zinc acetate

TGA-DTA study was carried out in the temperature range of 25–800 °C to understand the decomposition of zinc acetate (dihydrate) and thermal stability of ZnO. Figure 1 shows a typical TGA and DTA curves of zinc acetate (dihydrate). An endothermic reaction started initially corresponding to 19 % weight loss. This loss is due to the thermal dehydration of zinc acetate (dihydrate) to anhydrous zinc acetate [23]. Further decomposition of zinc acetate (anhydrous) was observed in the temperature range of 150–300 °C shows a second major weight loss of 61 % due to decomposition of acetate (More than the theoretical weight loss of 46.5 wt%). A 14.5 wt% difference might be

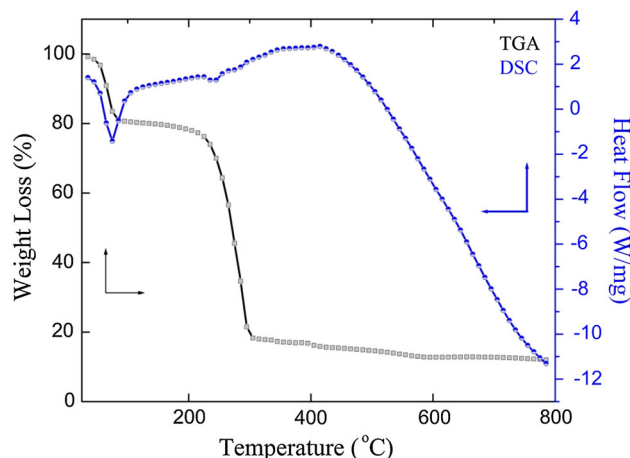
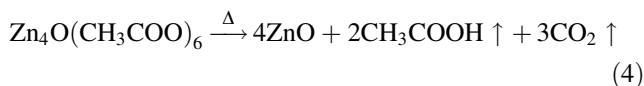
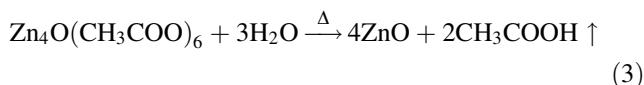
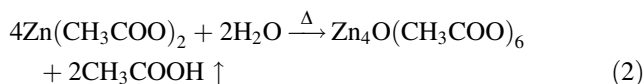
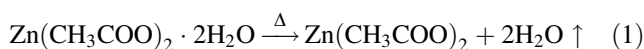


Fig. 1 TGA–DTA curves of zinc acetate dihydrate

due to the sublimation of zinc acetate species or the formation of other volatile organic zinc compounds such as $\text{Zn}_4\text{O}(\text{CH}_3\text{CO}_2)_6$ [24]. The ZnO formed by the following chemical reaction reported by Arii et al. [25].



3.2 Growth mechanism and morphology of ZnO

It is interesting to discuss the growth mechanism of ZnO nanowires, nanorods, spherical and irregular micro spherical morphology. The preferential growth of ZnO nanorods and nanowires at processing temperature 300 °C via thermal decomposition of zinc acetate dihydrate follows vapor solid growth mechanism, in this case the sublimation of material taking place before melting at normal pressure. In this process vapor generated from solid materials in the high temperature region is deposited onto a substrate at low temperature to form white ZnO nanorods. The gray color ZnO nanowires at the bottom of the crucible form in solid phase mechanism [26, 27]. Shakti et al. [28] reported recently growth mechanism based on the kinetics of crystal growth, the probability of nucleation on the surface of the whisker is given by.

$$P_N = B \exp\left(\frac{-\prod \sigma^2}{k^2 T^2 \ln \alpha}\right)$$

where P_N is nucleation probability, σ is the surface energy of the whisker, T is absolute temperature, α is the super saturation ratio ($\alpha = p/p_0$), where p is the actual vapor pressure and p_0 is the equilibrium vapor pressure corresponding to temperature T , k is the Boltzmann constant and B is the constant. Temperature and supersaturation ratio are the parameters that can be controlled by processing conditions. At low temperature (300 °C) and a small saturation ratio one dimensional nucleation is more favorable. This is an agreement with nanowires or nanorods like structure. At the 400 °C change in morphology like nanorods with an increase in diameter will occurs due to competition between the rate of nucleation and growth. At higher temperature (600 °C), the supersaturation ratio is more favorable for the nucleation resulting in spheres like growth, this is may be due to the nanorods diffusion into to sphere likes structures. Finally, at 800 °C, the species gets enough energy to diffuse and attain its favorable minimum energy state to form elongated irregular spheres [29]. The higher temperature of calcination promotes the disorder movement of the particles of host [24].

3.3 XRD analysis of ZnO prepared at different calcination temperature

XRD patterns of ZnO samples synthesized at different calcination temperature 200, 300, 400, 600 and 800 °C are designated as Z, Z_{1a}, Z_{1b}, Z₂, Z₃ and Z₄, respectively which is shown in Fig. 2. The XRD pattern observed at 200 °C relatively shows a less intense peak of ZnO and some other peaks of zinc acetate. When the calcination temperature increases from 300 to 800 °C for 3 h, all the diffraction peaks were observed at [100], [002], [101], [102], [110], [103], [201], [112] and [200] planes which are well

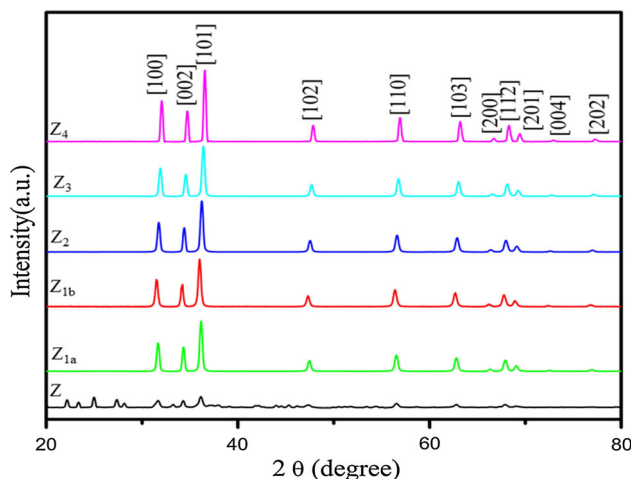


Fig. 2 XRD pattern of nanostructure ZnO samples Z, Z_{1a}, Z_{1b}, Z₂, Z₃ and Z₄ synthesized at different temperatures

indexed to a hexagonal wurtzite structure of ZnO and consistent with JCPDS 36-1451 [30]. No any other peaks were observed, which indicates the synthesized ZnO nanostructures are in pure phase. Hence the XRD results showed the conversion of zinc acetate (dihydrate) into ZnO. The crystallite size was calculated by using well known Scherrer's equation [31]. An average crystallite size was found to be 22, 26, 29, 35 and 40 nm for samples Z_{1a}, Z_{1b}, Z₂, Z₃ and Z₄, respectively. The lattice parameter and values of d were also calculated from the Bragg's equation ($n\lambda = 2d \sin\theta$), the lattice constants a , b , c and the primary cell volume were calculated from the lattice geometry equation and shown in Table 1 [32]. It was observed that as the calcination temperature increases a small change in the lattice parameter take place. This change in lattice parameter can be ascribed to the change of particle size due to quantum size effect [33]. The reduction of 'd' spacing value may be an indication of the high strain created in lattice due to calcination at higher temperature. Shidpour et al. [34] have reported most useful factor is the ratio of [002] polar plane to [100] non polar plane that can be related to the photocatalytic activity. It is found that the polar planes of ZnO are important for the activity, higher is the ratio more will be the photocatalytic activity of ZnO nanorods synthesized at 300 °C. The lattice parameter, cell volume and ratio of the plane of the ZnO nanomaterials calcined at different temperatures are summarized in Table 1.

3.4 SEM and EDS analysis

The surface morphology of ZnO samples Z_{1a}, Z_{1b}, Z₂, Z₃ and Z₄, obtained at different temperature was scanned by using SEM and shown in Fig. 3. The sample calcinated at 300 °C shows two kinds of color, the white powder (Z_{1a}) covered on the wall of crucible had nanorods morphology, while gray (Z_{1b}) powder stuck to the bottom of crucible had nanowires like morphology. The temperature raised to 400 °C, the ZnO nanorods (Z₂) was obtained with large diameter compared to Z_{1a}. This can be explained at lower temperature from 300 to 400 °C 1 D growth is favorable. Further increase in the temperature to 600 °C, morphology of ZnO (Z₃) is found to be spherical and at 800 °C, the morphology of ZnO (Z₄) was large size irregular micro-sphere because of higher temperature the growth species get enough energy to diffuse and attain their minimum energy shape i.e. spherical or micro spherical. Hence, the surface morphology of ZnO was found to be greatly influenced by calcination temperature.

Figure 4 shows the energy dispersive X-ray spectroscopic (EDS) analysis of a representative sample (Z_{1a}) calcined at 300 °C was used to investigate the elements present in the material. The spectrum consists of peaks

Table 1 Structural parameters of ZnO nanostructure synthesized at different temperature

ZnO samples calcined at different temperatures	Z _{1a}	Z _{1b}	Z ₂	Z ₃	Z ₄
Average crystallite size in nm	22	26	29	35	40
Lattice parameter Å	a = 3.2774 c = 5.2446	a = 3.2616 c = 5.22420	a = 3.2547 c = 5.2128	a = 3.2513 c = 5.2068	a = 3.2376 c = 5.1886
c/a	1.6002	1.6017	1.6016	1.6026	1.6015
Volume (Å) ³	48.7842	48.1293	47.8207	47.099	47.00
d Å	2.4936	2.48364	2.4787	2.467	2.45
Angle in degree	36.0180	36.167	36.24	36.40	36.60
Intensity ratio = 002/100	0.8571	0.8242	0.8237	0.7834	0.7570

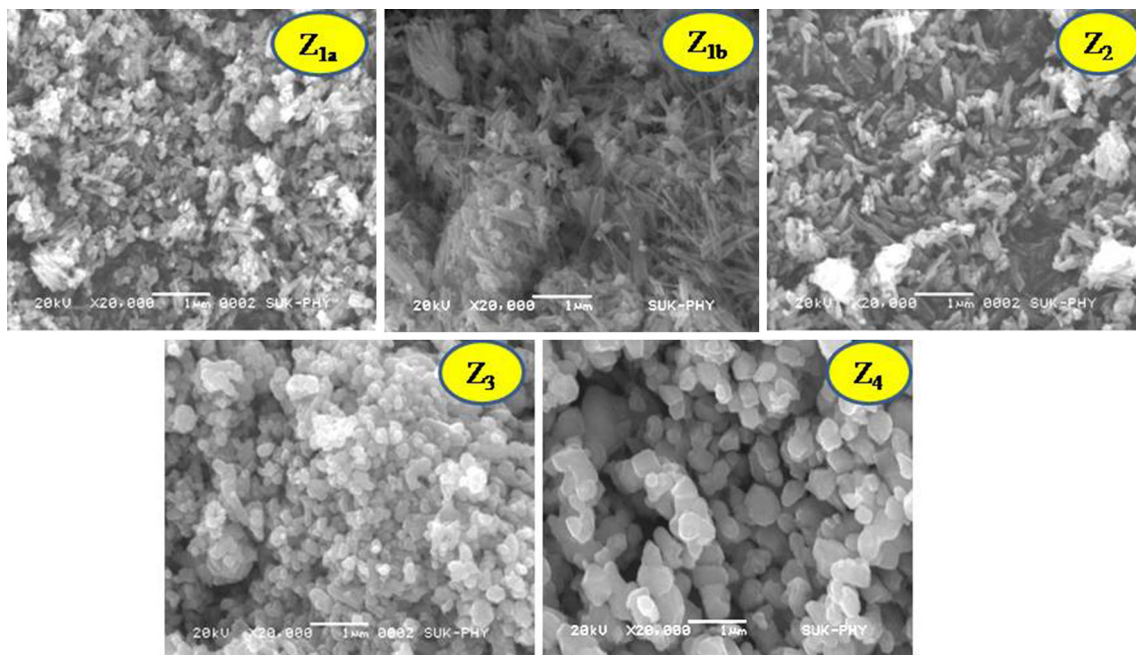


Fig. 3 SEM images of nanostructure ZnO samples Z, Z_{1a}, Z_{1b}, Z₂, Z₃ and Z₄ synthesized at different temperatures

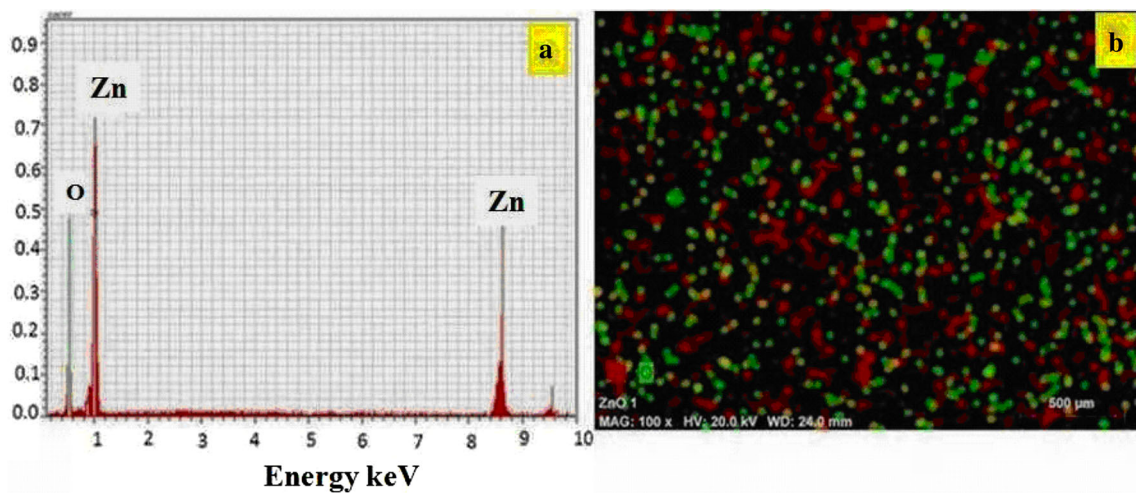


Fig. 4 EDS spectrum (a) and mapping image (b) of ZnO nanorods (Z_{1a}) calcined at 300 °C

corresponding to elements zinc and oxygen. No other peaks were observed from EDS, which confirms that the as-synthesized ZnO nanorods are in pure form.

3.5 TEM and HR-TEM images of ZnO nanorods

A representative TEM image of ZnO nanostructure (Z_{1a}) prepared at 300 °C is shown in Fig. 5a and b which shows rod shaped morphology. From the TEM image, it is observed that nanorods are not uniform in size. The diameter of the nanorods is in the range of 20–25 nm and the average length is found to be 400 nm. The HR-TEM image is shown in Fig. 5c, which shows ‘d’ spacing of 0.26 nm, corresponding to the [002] plane that indicating the ZnO nanorods are crystalline with hexagonal wurtzite structure [35]. Selected area electron diffraction (SAED) is presented in Fig. 5d, which shows dotted concentric rings that can be assigned to crystalline form.

3.6 FT-IR

FT-IR spectra in the range of 4000–400 cm^{-1} for zinc acetate dihydrate calcinated at different temperatures are shown in Fig. 6. At 200 °C temperature, bands were observed at 1580 and 1401 cm^{-1} in the spectrum due to asymmetric and symmetric stretching vibrations of (COO–Zn) of zinc acetate [36]. The broad band observed in the 3440 cm^{-1} region corresponds to the stretching vibration of the O–H band due to the adsorbed water [37]. The intensity of band due to the OH and carbonyl group get reduced as the calcination temperature increases. From 300 to 400 °C the band observed around 440–490 cm^{-1}

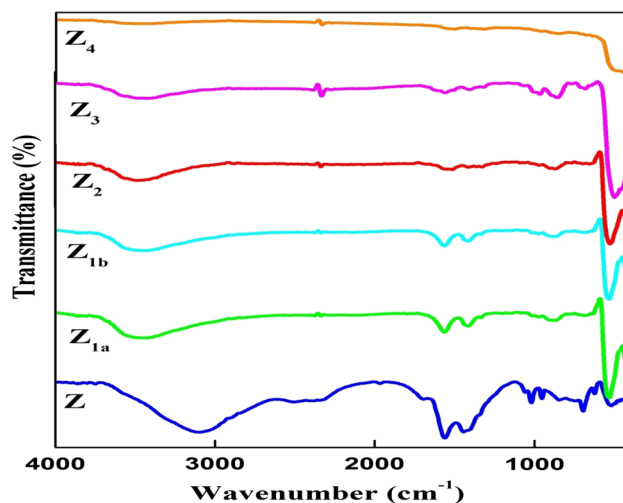
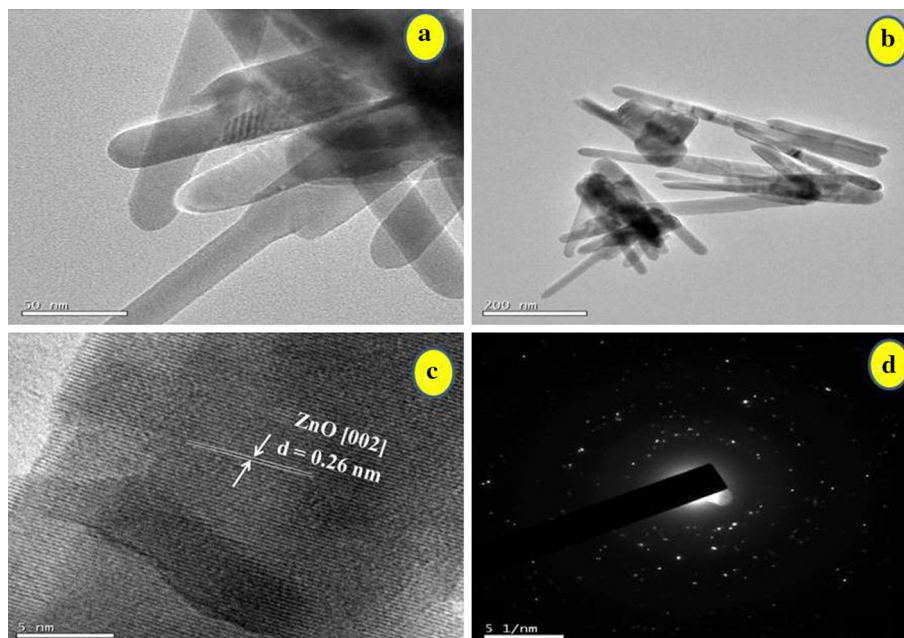


Fig. 6 FT-IR spectra of nanostructure ZnO samples Z, Z_{1a} , Z_{1b} , Z_2 , Z_3 and Z_4 synthesized at different temperatures

corresponds to the asymmetric stretching mode of wurtzite ZnO band and 501–550 cm^{-1} region corresponds to the symmetric stretching mode of Zn–O bond [26]. Further increase in calcination temperature from 600 to 800 °C, these two peaks are merged into a single peak corresponds to vibrational band observed at 489 cm^{-1} for Zn–O [38], this may be due to the change in morphology of ZnO from nanowires and nanorods to spherical shape. Thus FT-IR can be used not only for qualitative characterization but also confirmation of the shape of ZnO nanostructure similar results were reported [39, 40].

Fig. 5 a, b TEM images of ZnO (Z_{1a}) calcinated at 300 °C, c HRTEM and d SAED pattern



3.7 UV–Vis. Diffuse reflectance spectra of ZnO nanostructure

The UV–Vis. diffuse reflectance spectra of ZnO nanostructures obtained at different calcination temperatures (300, 400, 600 and 800 °C) are shown in Fig. 7a. From the figure it is seen that the absorption edges were red shifted possibly due to increase in particle size with increase in the calcination temperature [41]. The band gap energy is an important for the photocatalytic activity because the energy of incident light must be greater than or equal to the band gap energy. Therefore, the optical band gap with direct transition can be calculated from the following equation [42]

$$(\alpha h\nu) = A (h\nu - E_g)^{1/2}$$

where α , ν , A , and E_g are the absorption coefficient, frequency, proportionality constant and band gap energy respectively. The $(\alpha h\nu)^2$ against the $h\nu$ was plotted and the band gap was obtained by extrapolating the straight line to the $h\nu$ axis, which is shown in Fig. 7b. The band gap values of ZnO are found to be 3.38, 3.31, 3.29, 3.27 and 3.23 eV, for the different samples Z_{1a} , Z_{1b} , Z_2 , Z_3 and Z_4 , respectively. The band gap is thus found to be decreased from 3.38 to 3.22 eV. This might be due to change in their morphology, particle size and surface microstructures as a function of calcination temperature.

3.8 Photoluminescence of ZnO nanostructures

The PL is the emission of light that originates from the radiative recombination of photogenerated electrons and

hole pairs [43]. The room temperature PL spectra of ZnO nanostructure prepared at different calcination temperatures were measured at an excitation wavelength of 325 nm and shown in Fig. 8. Two emission bands could be observed for these five samples. The emission at around 380–400 nm is the characteristic near-band-edge emission due to the recombination of free photogenerated electrons and holes [44] and the other one is a deep-level emission mostly in the green region (471 nm), which is produced by the transition of excited optical centers from the deep level to the valence level, such deep-level emission being usually accompanied by the presence of structural defects [19, 45]. The red-shift of UV emission was observed from 390 to 412 nm due to the increase in size of the particles [46, 47]. It is well known that the photo-generated electron–hole pairs recombine, the photocatalytic activity would be decreased, higher the PL intensity lower the life time for photogeneration of electron hole pairs [48]. Among all the samples, the intensity of emission peak was the lowest for ZnO nanorods obtained at 300 °C, indicating that the longest life time of photo excited electron–holes [49, 50]. The most efficient separation of electron–hole pairs for sample Z_{1a} as compared to other samples, which might be results into a higher photocatalytic activity.

3.9 Photocatalytic degradation of acid green 25

3.9.1 Effect of calcination temperature

Photocatalytic degradation (PCD) efficiency of ZnO mainly depends on morphology and particle size of the photocatalyst [51]. Morphology and particle size of ZnO

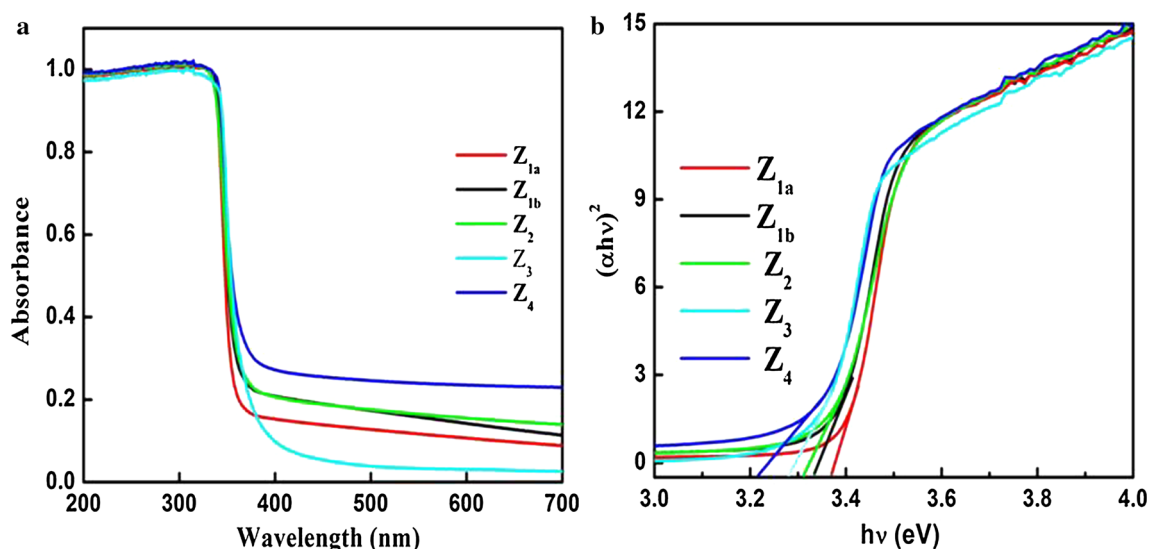


Fig. 7 **a** UV–Vis diffuse reflectance spectra and **b** Tauc plot nanostructure ZnO samples Z_{1a} , Z_{1b} , Z_2 , Z_3 and Z_4 synthesized at different temperatures

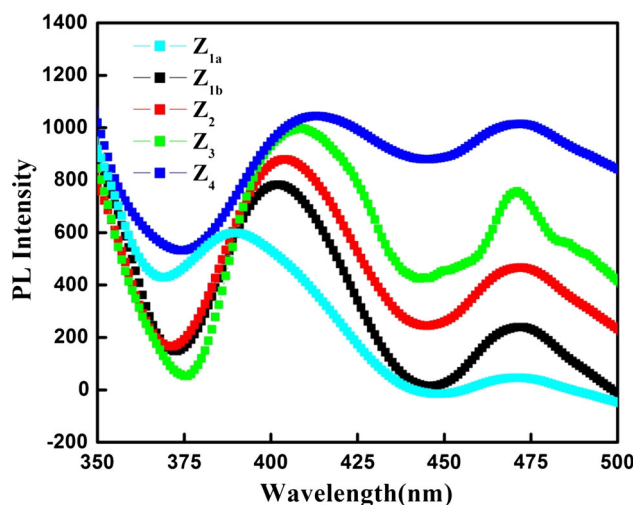


Fig. 8 PL spectra of nanostructure ZnO samples Z_{1a} , Z_{1b} , Z_2 , Z_3 and Z_4 synthesized at different temperatures

have been changed (nanowires, nanorods, spherical and irregular microspheres) by varying the calcination temperature from 300 to 800 °C (Fig. 9). The PCD efficiency of ZnO formed at 300 to 800 °C was investigated for AG-25 under UV light. The ZnO nanorods obtained at 300 °C (Z_{1a}) showed maximum 99 % photocatalytic degradation within 60 min. This higher photodegradation is attributed to ZnO nanorod shaped morphology offers several advantages such as decreased grain boundaries, having the highest separation rate of electron hole pairs, smaller crystallite size and higher relative ratio of polar [002] to non polar plane [100]. Earlier, Shidpour et al. [34] reported that higher is the ratio better is the photocatalytic activity. After an increase in calcination temperatures from 400 to 800 °C, the PCD efficiency of ZnO was found to be

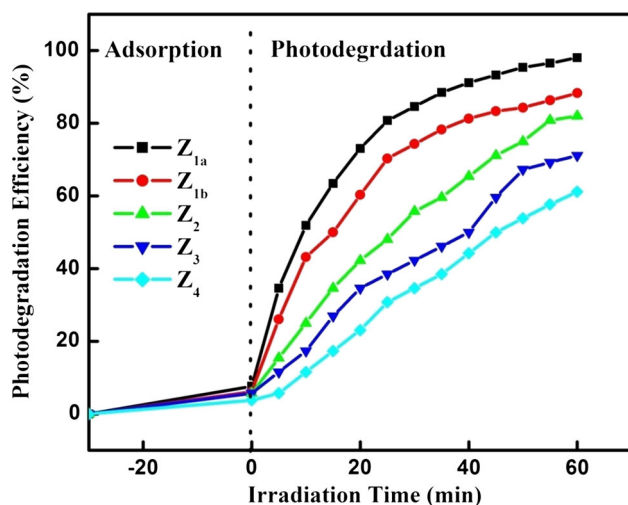


Fig. 9 Effect of calcination temperature on photodegradation efficiency of Z_{1a} , Z_{1b} , Z_2 , Z_3 and Z_4 towards AG-25

decreased from 82 to 61 %. This may be due to the fact that with the increase in calcination temperature, morphology changes to spherical and crystallite size of ZnO also increases, therefore the surface area decreases, which results into the decrease in the active sites of the photocatalyst for adsorption of substrate molecules [52]. Thus size and morphology of as-synthesized ZnO is affecting PCD efficiency. The calcination temperatures were increased beyond 600 °C, at the same time; particle size was greatly increased and shows irregular micro spherical morphology, which shows the negative effect on PCD efficiency (Fig. 8). The most photocatalytic active ZnO nanorods forms at 300 °C, therefore we have selected 300 °C as an optimum calcination temperature to study other parameters such as loading of photocatalyst and pH.

3.9.2 Effect of catalyst loading

Photocatalysis is heterogeneous in nature and its photodegradation efficiency depends on concentration of reactant and active sites of the photocatalyst. It is essential to find out optimum amount of catalyst loading in order to avoid excess use of the photocatalyst. The effect of ZnO nanorods (Z_{1a}) loading on the degradation of the AG-25 (25 ppm) dye under UV illumination has been examined by varying the catalyst amount from 0.5 to 2 g/dm³ by keeping other parameters identical. The results are shown in Fig. 10 which indicates that the initially increase in catalyst loading from 0.5 to 1.5 g/dm³ increase in degradation efficiency from 83 to 99 % within 35 min. It is seen that the degradation efficiency increases with increase in the amount of catalyst loading, which is attributed to the increase in the number of active sites and more active sites

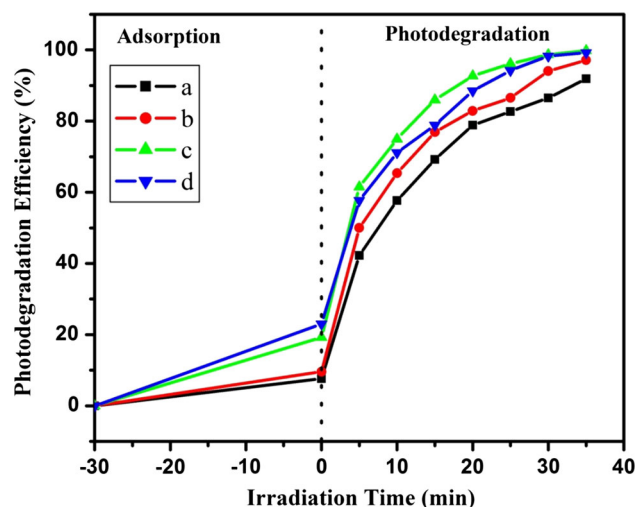


Fig. 10 Effect of catalyst loading a 50, b 100, c 150 and d 200 mg/100 mL on photodegradation efficiency of ZnO nanorods (Z_{1a}) for AG-25

will provide more chances to receive both the light and guest molecules [48, 53]. A further increase in the catalyst loading does not affect the degradation efficiency significantly. This observation can be explained in terms of availability of active sites for photocatalytic reactions. It was found that large amount of catalyst may result in the agglomeration of catalyst [54]. Another reason for the decreased degradation efficiency is the turbidity of suspension and this leads to decrease in penetration of UV light and hence activity of photocatalyst decreases [55].

3.9.3 Effect of pH

The pH of the AG-25 solution also plays an important role in the photodegradation process. This can affect for the degradation rate, therefore pH effect needs to be investigated. The effect of pH on the photocatalytic degradation of AG-25 was studied in the pH range 3–11. The results of pH effects are illustrated in Fig. 11. It was observed that the degradation efficiency increases with increase in pH, exhibiting maximum degradation efficiency (99 %) at pH 7 and further increase in the pH decrease in degradation efficiency was observed. The height degradation is may be due to the zero point charge for ZnO (9.0) and above this value, the ZnO surface is predominantly negatively charged, which can affect the electrostatic repulsion between anionic AG-25 and photocatalyst which inhibits adsorption of the dye on the photocatalyst [56]. In acidic medium the degradation efficiency was less, this may be due to dissolution of ZnO at lower pH [57]. It appears that a low efficiency of degradation (50 %) was found to be at pH 3 due to dissolution of ZnO in the acidic environment [58].

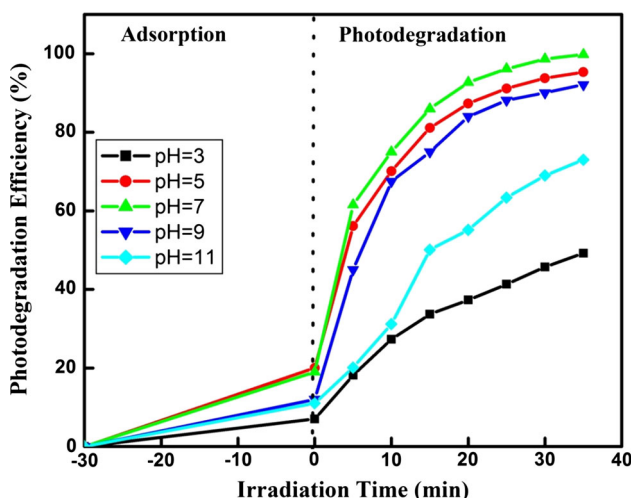


Fig. 11 Effect of pH on photodegradation efficiency of ZnO nanorods (Z_{1a}) for AG-25

Figure 12 shows the UV–Vis spectra of the AG-25 solution after 35 min under UV light in the presence of ZnO nanorods (1.5 g/dm³ at pH = 7.) The spectra corresponding to the double bands in the visible region with absorbance maxima at 609 and 643 nm and the latter at 409 nm are due to the AG-25. The band in the UV region are localized at 254 and 284 nm are attributed to benzene cycle substituted by SO₃²⁻ [59]. In the present study, all absorbance band gets decreased which indicates that complete mineralization occurs.

3.9.4 Comparison of ZnO with Degussa P25 TiO₂

For the sake of comparison, the photocatalytic activity of ZnO nanorods synthesized at 300 °C and Degussa P25 were evaluated under the reaction conditions (pH = 7, 1.5 g/dm³ and AG-25 at 25 ppm) as shown in Fig. 13. The experimental result reveals that as-synthesized ZnO nanorods are found to be more efficient than TiO₂ (P25) towards the degradation of AG-25. The ZnO nanorods show 99 % photodegradation efficiency under UV light whereas in presence of TiO₂ (P25) 87 % within 35 min. The better photocatalytic activity of ZnO nanorods compared to P25 is mainly due to positively charged ZnO surface at pH = 7 which helps to adsorb anionic AG-25 more efficiently than that of TiO₂ (P25). The other reason of better photocatalytic activity is the one-dimensional ZnO nanorods material offers several advantages over nanoparticles, including high surface-to-volume ratio, enhancement of light absorption and rapid diffusion of reactive species transport along the long direction [60].

In addition to the photodegradation experiments, the several control experiments were carried out to ensure the

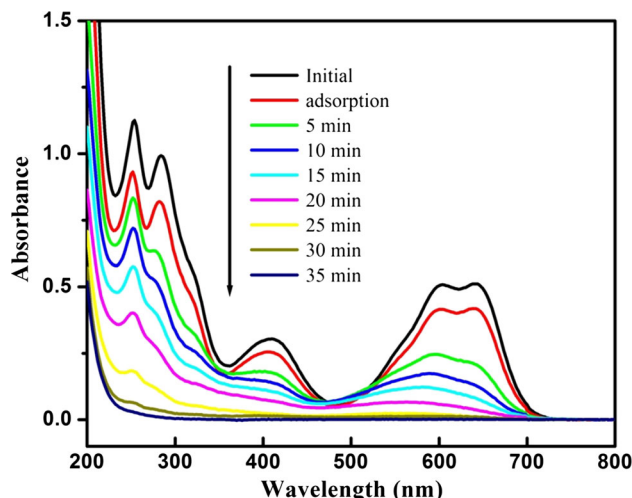


Fig. 12 UV-Visible absorption spectra of degradation of AG-25(25 ppm) under UV light in presence of ZnO nanorods

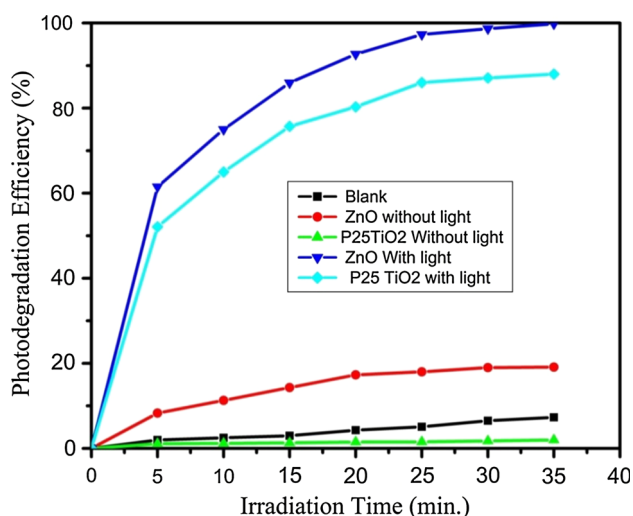


Fig. 13 Comparison the photodegradation efficiency of as-synthesized ZnO nanorods (Z_{1a}) with TiO_2 (P25)

decrease in concentration of dye mainly due to the photocatalytic activity. The control experiments are direct photolysis, adsorption of AG-25 on the surface of ZnO nanorods and TiO_2 (P25) were carried out. The experimental results of these studies are given in Fig. 13 which shows that direct photolysis did not cause any significant degradation (2 %) under UV irradiation. In the presence of ZnO without irradiation (19 % adsorption), slight decrease in the concentration of AG-25 was observed, this may be due to the adsorption of the anionic dye on the surface of ZnO nanorods. In presence of Degussa P25 adsorption is (1 %) negligible compared to ZnO nanorods.

The reusability of the photocatalyst is one of the most important parameter for its practical and commercial applications. The ZnO nanorods can be easily recovered by centrifugation and reused. To study the reusability of the ZnO nanorods, four successive photocatalytic runs were carried out by adding recycled ZnO nanorods to fresh AG-25 solutions. The photocatalytic activity obtained for recycled ZnO was shown in Fig. 14. There is no significant change was observed in the activity even after the fourth successive cycle. Therefore, the ZnO nanorods show high-performance with potential applications in environmental remediation.

3.9.5 Chemical oxygen demand (COD)

COD is widely used as an effective technique to measure the strength of the mineralization of organic content. The percentage removal of COD of the AG-25 before and after photocatalysis was estimated at optimized conditions (25 ppm AG-25, 1.5 g/dm^3 ZnO nanorods and $\text{pH} = 7$ under UV light). It can be seen that considerable reduction

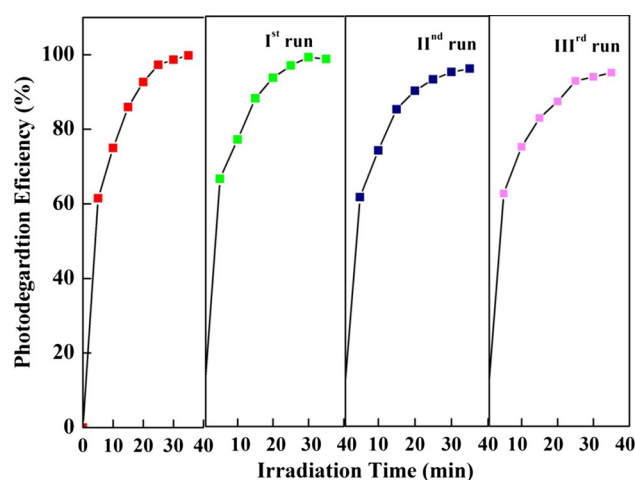


Fig. 14 Photodegradation of AG-25 by ZnO nanorods (Z_{1a}) for four runs

of the COD from 49 to 7 mg/dm^3 was obtained within 35 min. This result indicates 85 % mineralization of the AG-25.

3.9.6 LC-MS for identification of photodegradation products

Photodegradation reactions are often complex, that follows various competing or parallel pathways and leading to multiple unaccepted reaction products [61]. Therefore, the elucidation of photodegradation pathways and identification of transformed products are of crucial interest to understand their fate in the aquatic environment. Hence, we have carried out LC-MS analysis of photodegraded product of AG-25 and investigated the intermediate product and probable route of fragmentation of AG-25. The probable fragmentation route is shown in Fig. 15. The molecular ion peak at m/z 599 corresponds to AG-25 $[M-2H + Na]^-$. The AG-25 fragmentation proceeds through loss of methyl amino benzene sulphonate that gives the intermediate at m/z 186. After demethylation the amino sulphonate is formed at $m/z = 172$. Afterwards degradation proceeds to deamination and desulphonation. The above breaking of AG-25 molecules suggested by the presence of peaks at m/z 599, 379, 194, 186, 180, 173, 172, 157, 103 and 97. Thus m/z spectral data indicate the presence of some organic moieties in decolorization of AG-25. Formation of SO_3Na and HSO_4^- at m/z 103 and 97 respectively confirms the mineralization of the AG-25.

3.10 Antimicrobial activity

The antimicrobial activity of synthesized ZnO nanostructures was determined by pour plate agar well diffusion

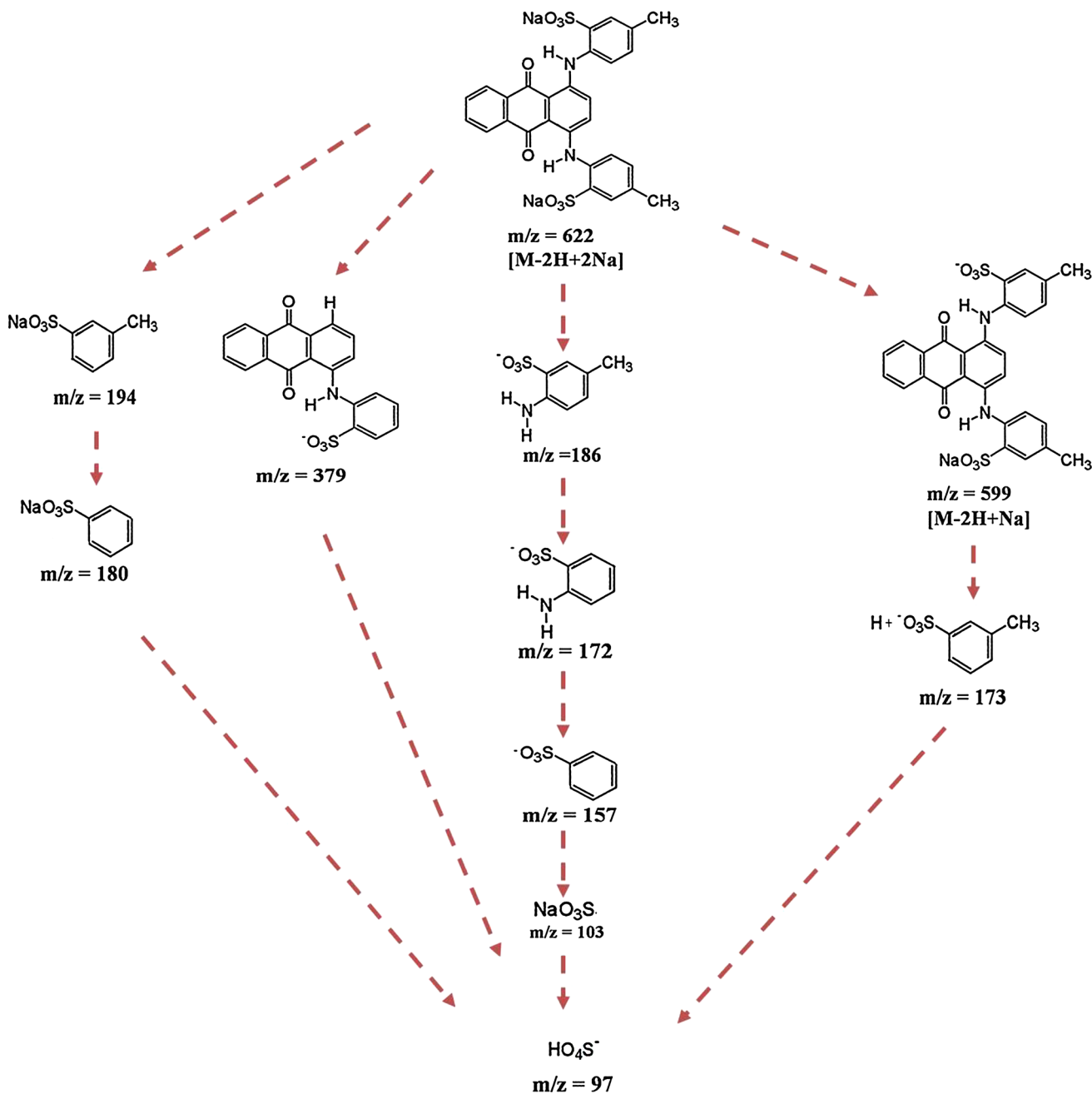


Fig. 15 Plausible photodegradation path for AG-25 using LC-MS

method and shown in Fig. 16. Each of the five kinds of ZnO samples such as nanowires, nanorods, spherical and micro irregular spherical were obtained at different calcination temperatures. In our experiment, we have used the 1 mg/mL as a stock solution of ZnO, further dilutions are made by water to 1:1, 1:2 and 1:3. It is clear that as the dilution increases the zone of inhibition get reduced. The maximum zone of inhibition at 1 mg/mL for ZnO obtained at each calcinations temperature. The zones of inhibition diameters were measured and summarized in Table 2. In

the present study, the sample Z_{1a} and Z_{1b} that exhibits better antimicrobial activity than the sample Z_2 , Z_3 and Z_4 . From the plate assay, it is observed that the control experiment (absence of ZnO) shows no inhibition zones of bacterial growth.

The formations of zones around the samples demonstrate nanostructures of ZnO that can effectively prevent the growth of these bacteria. This might be due to the direct interaction between nanostructures of ZnO and membrane surface of the bacterial cell causing disruption of the cell

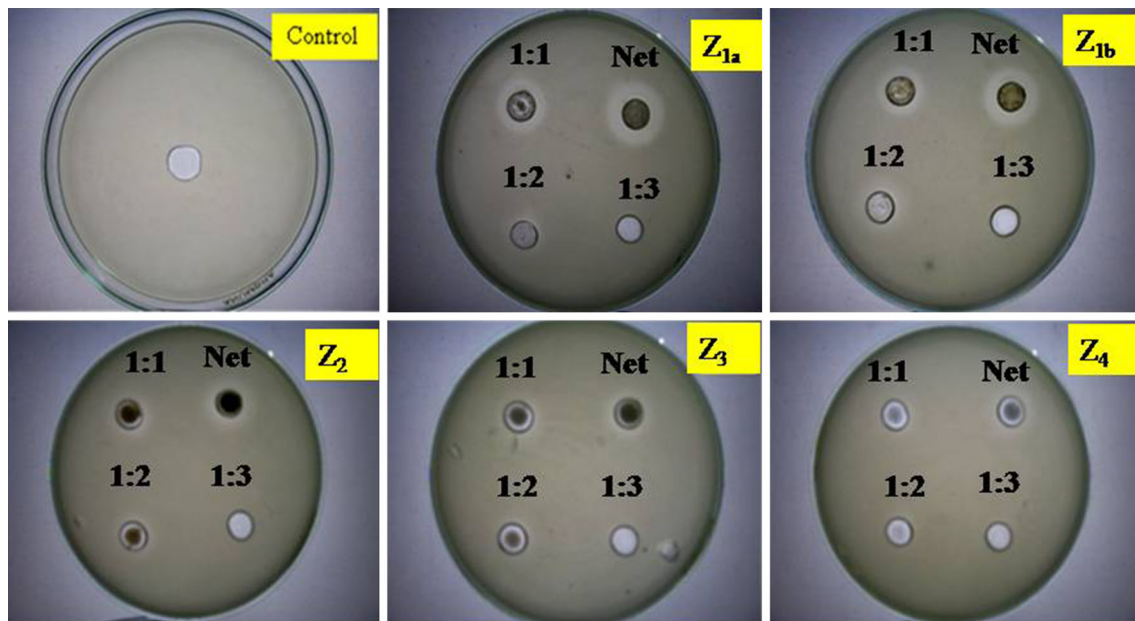


Fig. 16 Antimicrobial activity of ZnO nanostructures (Z_{1a} , Z_{1b} , Z_2 , Z_3 and Z_4) against *E. Coli*

Table 2 Antimicrobial activity of ZnO nanostructures for *E.coli*

Sample code	Calcination temperature (°C)	Antimicrobial activity (zone of inhibition in mm) 1 mg/mL	Antimicrobial activity (zone of inhibition in mm)			Antimicrobial activity (zone of inhibition in mm) control
			1:1	1:2	1:3	
Z	200	–	–	–	–	–
Z_{1a} white	300	13	9	5	0	0
Z_{1b} gray	300	12	8	3	0	0
Z_2	400	7	5	3	0	0
Z_3	600	5	4	3	0	0
Z_4	800	4	3	2	0	0

membrane of the bacteria. It was found that the antimicrobial activity of ZnO calcined at 300 °C showed significantly higher inhibition efficiencies than the other samples, these can be ascribed to the smaller crystallite size with nanorods and the nanowire morphology of the ZnO obtained at calcined 300 °C.

4 Conclusions

In the present work, ZnO nanostructures have been synthesized with different morphology by solid state thermal decomposition method which is a simple, rapid cost-effective and can be applicable for large-scale production. The morphology, photocatalytic and antimicrobial activities of the resulting ZnO catalysts can be changed by just changing the calcination temperature. The experimental results reveal that ZnO nanorods synthesized at 300 °C

show excellent photocatalytic as well as antimicrobial activity. The enhancement in the photocatalytic as well as antimicrobial activity of ZnO nanorods obtained at 300 °C, due to small crystallite size, high surface area and more charge separation. The highest (99 %) photocatalytic degradation of AG-25 was achieved at optimal condition (pH = 7, 25 ppm dye, ZnO nanorods 1.5 g/dm³) within 35 min. under UV illumination. As-synthesized ZnO nanorods found to be more efficient than TiO₂ (P25) towards the degradation of AG-25. In addition to that ZnO photocatalyst was easily recovered and its efficiency was found to be stable even after four runs. The mineralization of dye was confirmed by COD. The AG-25 fragmentation proceeds by loss of methyl amino benzene sulphonate that gives the intermediate at m/z 186. This method does not require special equipments i.e. the simplicity of the present method and considering the excellent photocatalytic as well as antimicrobial performance of ZnO nanorods

suggests its potential environmental cleaning applications at industrial scale.

Acknowledgments KMG acknowledges to DST for providing financial assistance under the Major Research Project (SR/S1/PC/0041/2010).

References

- M.H. Farzana, S. Meenakshi, *Ind. Eng. Chem. Res.* **53**, 55 (2014)
- Z. Xiong, A. Xu, H. Li, X. Ruan, D. Xia, Q. Zeng, *Ind. Eng. Chem. Res.* **52**, 362 (2013)
- P. Bansal, D. Singh, D. Sud, *Sep. Purif. Technol.* **72**, 357 (2010)
- Z. Shu, X. Jiao, D. Chen, *Cryst. Eng. Comm.* **15**, 4288 (2013)
- J. Xie, Y. Li, W. Zhao, L. Bian, *Powder Technol.* **207**, 140 (2011)
- M.B. Suwarnkar, R.S. Dhabbe, A.N. Kadam, K.M. Garadkar, *Ceram. Int.* **40**, 5489 (2014)
- J. Yu, X. Yu, *Environ. Sci. Technol.* **42**, 4902 (2008)
- Y. Peng, S. Qin, W. Wang, A.W. Xu, *Cryst. Eng. Comm.* **15**, 6518 (2013)
- S. Sakthivel, B. Neppolian, M.V. Shankar, B. Arabindoo, M. Palanichamy, V. Murugesan, *Sol. Energy Mater. Sol. Cells* **77**, 65 (2003)
- M. Premanathan, K. Karthikeyan, K. Jeyasubramanian, G. Manivannan, *Nanomed. Nanotechnol. Biol. Med.* **7**, 184 (2011)
- P.J.P. Espitia, N.F.F. Soares, R.F. Teofilo, D.M. Vitor, J.R. Coimbra, N.J. Andrade, F.B. Sousa, R.D. Sinisterra, E.A.A. Medeiros, *J. Nanopart. Res.* **15**, 1324 (2013)
- J. Becker, K.R. Raghupathi, J.S. Pierre, D. Zhao, R.T. Koodali, *J. Phys. Chem. C* **115**, 13844 (2011)
- L. Jing, Y. Qu, B. Wang, S. Li, B. Jiang, L. Yang, W. Fu, H. Sun, *Sol. Ener. Mater. Sol. Cells* **90**, 1773 (2006)
- N. Padmavathy, R. Vijayaraghavan, *Sci. Technol. Adv. Mater.* **9**, 1 (2008)
- S. Singh, K.C. Barick, D. Bahadur, *Cryst. Eng. Comm.* **15**, 4631 (2013)
- X. Cai, Y. Cai, Y. Liu, H. Li, F. Zhang, Y. Wang, *J. Phys. Chem. Solids* **74**, 1196 (2013)
- L. Song, S. Zhang, X. Wu, Q. Wei, *Ind. Eng. Chem. Res.* **51**, 4922 (2012)
- Z. Wang, X. Qian, J. Yin, Z. Zhu, *Langmuir* **20**, 3441 (2004)
- F. Su, X. Qiao, F. Tan, W. Wang, X. Qiu, *Appl. Surf. Sci.* **263**, 704 (2012)
- C. Tian, Q. Zhang, A. Wu, M. Jiang, Z. Liang, B. Jiang, H. Fu, *Chem. Commun.* **48**, 2858 (2012)
- L. Wang, C.G. Tian, B.L. Wang, R.H. Wang, W. Zhou, H.G. Fu, *Chem. Commun.* **44**, 5411 (2008)
- A.N. Kadam, R.S. Dhabbe, M.R. Kokate, Y.B. Gaikwad, K.M. Garadkar, *Spectrochim. Acta A Mol. Biomol. Spectro.* **133**, 669 (2014)
- C.C. Lin, Y.Y. Li, *Mater. Chem. Phys.* **113**, 334 (2009)
- R. Saravanan, E. Thirumal, V.K. Gupta, V. Narayanan, A. Stephen, *J. Mol. Liq.* **177**, 394 (2013)
- T. Arai, A. Kishi, *Thermochim. Acta* **400**, 175 (2003)
- M. Farbod, E. Jafarpour, *Ceram. Int.* **40**, 6605 (2014)
- M. Farbod, E. Jafarpour, *Mater. Lett.* **85**, 47 (2012)
- N. Shakati, P. Asit, T. Mandal, M. Katiyar, *Mater. Sci. Semicond. Process.* **20**, 55 (2014)
- Y. Zhang, M.K. Ram, E.K. Stefanakos, D.Y. Goswami, *J. Nanomater.* **2012**, 1 (2012)
- L. Yang, G. Wang, C. Tang, H. Wang, L. Zhang, *Chem. Phys. Lett.* **409**, 337 (2005)
- P.V. Korake, A.N. Kadam, K.M. Garadkar, *J. Rare Earth.* **32**, 306 (2014)
- A.K. Zak, M.E. Abrishami, W.H.A. Majid, R. Yousefi, S.M. Hosseini, *Ceram. Int.* **37**, 393 (2011)
- M. Hosokawa, K. Nogi, M. Naito, T. Yokoyama, *Nanopart. Technol. Handbook*, Elsevier, Amsterdam, 2007. 622 pp. Book 2007 ISBN:978-0-444-53122-3
- R. Shidpour, A. Simchi, F. Ghanbari, M. Vossoughi, *Appl. Catal. A General* **472**, 198 (2014)
- S. Wang, Z. Li, P. Wang, C. Xiao, R. Zhao, B. Xiao, T. Yang, M. Zhang, *Cryst. Eng. Comm.* **16**, 5716 (2014)
- A.V. Ghule, B. Lo, S.H. Tzing, K. Ghule, H. Chang, Y.C. Ling, *Chem. Phys. Lett.* **381**, 262 (2003)
- C.C. Li, X.M. Yin, Q.H. Li, T.H. Wang, *Cryst. Eng. Comm.* **13**, 1557 (2011)
- A.R. Mereu, A. Mesaros, T. Petrisor, M. Gabor, M. Mihai, M. Popa, L. Ciontea, *J. Anal. Appl. Pyrol.* **104**, 653 (2013)
- S. Music, D. Dragcevi, S. Popovic, *J. Alloys Compd.* **429**, 242 (2007)
- R. Velmurugan, M. Swaminathan, *Sol. Ener. Mater. Sol. Cells* **95**, 942 (2011)
- J. Lv, W. Gong, K. Huang, J. Zhu, F. Meng, X. Song, Z. Sun, *Superlattice Microst.* **50**, 98 (2011)
- S. Ilcan, Y. Caglar, M. Caglar, *J. Optoelectron, Adv. Mater.* **10**, 2578 (2008)
- R.S. Dhabbe, A.N. Kadam, M.B. Suwarnkar, M.R. Kokate, K.M. Garadkar, *J. Mater. Sci. Mater. Electron.* **25**, 3179 (2014)
- W. Sun, J. Li, G. Mele, Z. Zhang, F. Zhang, *J. Mol. Catal. A Chem.* **366**, 84 (2013)
- X. Li, J. Wang, J. Yang, L. Jinghai, M. Wei, M. Maobin, X.J. Meng, S. Lu, Y. Sui, *Mol. Catal. A Chem.* **378**, 1 (2013)
- T.M. Hammad, J.K. Salem, R.G. Harrison, *Superlattice. Microst.* **47**, 335 (2010)
- V.A. Fonoberov, A.A. Balandin, *Appl. Phys. Lett.* **85**, 5971 (2004)
- J. Yang, M. Gao, Y. Zhang, L. Yang, J. Lang, D. Wang, H. Liu, Y. Liu, Y. Wang, H. Fan, *Superlattice. Microst.* **44**, 137 (2008)
- X. Wang, Y. Zhang, C. Hao, F. Feng, H. Yin, N. Si, *Ind. Eng. Chem. Res.* **53**, 6585 (2014)
- A. Kajbafvala, H. Ghorbani, A. Paravar, J.P. Samberg, E. Kajbafvala, S.K. Sadmezhaad, *Superlattices Microst.* **51**, 512 (2012)
- S.K. Pardeshi, A.B. Patil, *J. Mol. Catal. A Chem.* **308**, 32 (2009)
- F. Lei, B. Yan, *J. Phys. Chem. C* **113**, 1074 (2009)
- A.N. Kadam, R.S. Dhabbe, M.R. Kokate, K.M. Garadkar, *J. Mater. Sci. Mater. Electron.* **25**, 1887 (2014)
- P.V. Korake, R.S. Dhabbe, A.N. Kadam, Y.B. Gaikwad, K.M. Garadkar, *J. Photochem. Photobiol. B Bio.* **130**, 11 (2014)
- N. Daneshvar, D. Salari, A.R. Khataee, *J. Photochem. Photobiol. A Chem.* **157**, 111 (2003)
- J. Wang, Z. Jiang, Z. Zhang, Y. Xie, X. Wang, Z. Xing, R. Xu, X. Zhang, *Ultrason. Sonochem.* **15**, 768 (2008)
- P. Amornpitoksuk, S. Suwanboon, S. Sangkanu, A. Sukhoom, J. Wudtipan, K. Srijan, S. Kaewtaro, *Powder Technol.* **212**, 432 (2011)
- E. Evgenidou, K. Fytianos, I. Poullos, *J. Photochem. Photobiol. A Chem.* **175**, 29 (2005)
- H. Hentit, M.R. Ghezzer, M. Womes, J.C. Jumas, A. Addou, M.S. Ouali, *J. Mol. Catal. A Chem.* **390**, 37 (2014)
- S. Lam, J. Sin, I. Satoshi, A.Z. Abdullah, A.R. Mohamed, *Appl. Catal. A General* **471**, 126 (2014)
- M. Petrovic, D. Barcelo, *Trends Anal. Chem.* **26**, 486 (2007)